Steel and Composite Structures, *Vol. 37, No. 1 (2020) 75-90*
DOI: https://doi.org/10.12989/scs.2020.37.1.075

Behavior of composite CFST beam-concrete column joints

Seung-Eock Kim[1], Ji-Hun Choi[1], Thai-Hoan Pham[2], Viet-Hung Truong[3], Zhengyi Kong[4],
Nguyen-Thê Duong[5] and Quang-Viet Vu*[6]

[1]*Department of Civil and Environmental Engineering, Sejong University, 98 Gunja-dong, Gwangjin-gu, Seoul, 05006, South Korea*
[2]*Department of Concrete Structures, National University of Civil Engineering, 55 Giai Phong, Hanoi, Vietnam*
[3]*Faculty of Civil Engineering, Thuyloi University, 175 Tay Son, Dong Da, Hanoi, Vietnam*
[4]*School of Civil Engineering and Architecture, Anhui University of Technology, Ma'anshan 243032, China*
[5]*Faculty of Civil Engineering, Duy Tan University, 03 Quang Trung, Da Nang, Vietnam*
[6]*Faculty of Civil Engineering, Vietnam Maritime University, 484 Lach Tray Street, Hai Phong city, Vietnam*

(*Received October 6, 2019, Revised September 11, 2020, Accepted September 11, 2020*)

Abstract. This paper introduces a new composite joint, which is the composite CFST beam- concrete column joint, and it is more convenient for transportation and erection than conventionally welded joints. The main components of this joint include steel H-beams welded with CFST beams, reinforced concrete columns, and reinforced concrete slabs. The steel H-beams and CFST beams are connected with a concrete slab using shear connectors to ensure composite action between them. An experimental investigation was conducted to evaluate the proposed composite joint performance. A three-dimensional (3D) finite element (FE) model was developed and analyzed for this joint using the ABAQUS/explicit. The FE model accuracy was validated by comparing its results with the relevant test results. Additionally, the parameters that consisted of the steel box beam thickness, concrete compressive strength, steel yield strength, and reinforcement ratio in the concrete slab were considered to investigate their influence on the proposed joint performance.

Keywords: concrete-filled steel tubular; composite joints; finite element model; ABAQUS/explicit

1. Introduction

CFST members, which include a steel hollow section and a concrete infill, have the benefits of both concrete and steel. The utilization of these members can reduce the construction time and enhance the seismic performance because of their high stiffness, high strength, ductility, and large energy absorption. As a result, they have recently been widely used in low-rise buildings as beams and in high-rise buildings as columns and beam-columns (Han *et al.* 2004, 2010, Tao and Han 2006, Moon *et al.* 2012, Esfandyary *et al.* 2015, Hassan *et al.* 2016, Thomas and Sandeep 2018, Yuan *et al.* 2019, Eom *et al*. 2019). Regarding the CFST columns used in beam-to-CFST column joints, research related to this joint have been extensively investigated through experimental tests, finite element analyses, (FEA) and analytical approaches (Elremaily and Azizinamini 2001, Wang *et al.* 2009a, b, Hassan *et al*. 2014, Yang *et al.* 2015, Li *et al.* 2018). Wang *et al.* (2009a) conducted an experimental study involving bolted moment connection joints of square or circular CFST columns and steel-H beams using high-strength blind bolts subjected to monotonic loading. Yang *et al.* (2015) investigated the rotational behavior of a simply bolted I-beam to a concrete-filled elliptical steel tubular column joints through an experimental approach. By performing experimental and numerical analysis, Wang *et al.* (2009b) examined the mechanical behavior of blind bolted end plate joints to concrete-filled thin-walled steel tubular columns, and they suggested that an innovative blind bolted joint could be applied in low-rise and mid-rise buildings. More recent work on composite beam-to-CFST column joints have been extensively implemented (Loh *et al*. 2006, Ataei *et al.* 2015, 2016, Thai and Uy 2015, Thai *et al.* 2017, Wang *et al.* 2018, Waqas *et al.* 2019, Guo *et al*. 2019, Ye *et al*. 2019). Among these researches, Ataei *et al.* (2015, 2016) conducted experimental studies of the flush end plates and high strength steel flush end plates beam-to-column composite joints with deconstructable bolted shear connectors. The proposed composite joint could be easily deconstructed at the end of its service life, the demolition waste was minimized, and the components recycling was maximized. Based on the research results, they also proposed the utilization of precast slabs in the composite joint to improve the quality of construction, reduce the construction time, and reduce labor costs. Thai *et al.* (2017) investigated the structural performance of blind bolted end plate composite joints to the square and circular CFST columns, and they suggested an analytical model to predict the moment-rotation behavior of the composite joint. By performing experimental and numerical studies, Waqas *et al.* (2019) examined the behavior of composite beam-to-CFST column flush end plate connections utilizing blind bolts subjected to static and cyclic loading. Based on the experimental results, they proved that the proposed joint could enhance the strength and stiffness compared with the previous studies. More recently, Guo *et al*. (2019)

*Corresponding author, Ph.D.
E-mail: vietvq@vimaru.edu.vn

ISSN: 1229-9367 (Print), 1598-6233 (Online)

Table 1 Details of the specimen

No	Member	Dimensions(mm)
1	Concrete column	500x500x1210 mm
2	Concrete slab	5200x2675x160 mm
3	Steel box beam	390x500x10 mm
4	Concrete filled steel tubular beam	370x480x2185 mm
5	Headed shear studs	M25x100 mm
6	Longitudinal reinforcing bars in slab	N16
7	Transverse reinforcing bars in slab	N19
8	Diagonal reinforcing bars in slab	N19
9	Internal reinforcing bars in column	N29
10	Stirrup	N10
11	Steel H-beam	H 390x300x10 mm
12	End plate	390x350x20

Table 2 Material properties for steel and concrete

No	Type of steel	Thickness/ Diameter	Yield strength F_y (MPa)	Ultimate strength, F_u (MPa)	Elastic modunlus, E_s (MPa)	Elongation (%)
1.	Flanges of steel box beam	10 mm	405.4	554.6	200,000	24
2.	Web of steel box beam	8 mm	414	548	200,000	25
3.	Longitudinal reinforcing bars	D16	547	670	200,000	16.3
4.	Transverse reinforcing bars/ Diagonal reinforcing bars	D19	545	671	200,000	15.4
5.	Internal reinforcing bars in column	D29	568	698	200,000	17.3
6.	Stirrup	D10	525	646	200,000	14.0
7.	Flanges of steel H-beam	16 mm	407	540	200,000	27
8.	Web of steel H-beam	10 mm	405.4	554.6	200,000	24
9.	End plate	20 mm	359	544	200,000	25
No	Specimen	Compressive Strength, f_{ck} (MPa)	Compressive strain, ε_c	Tensile strength, f_{tk} (MPa)	Tensile displacement, (mm)	
1.	Concrete slab/Concrete filled steel tubular beam	40.45	0.0028	3.89	2 mm	

investigated the seismic performance and failure mechanism of the CFDST column blind bolted to composite beam joint with partial shear interaction. From their results, they proposed calculation models to inspect the mechanical behavior of the this connection. Regarding the behavior of this joint under fire, Ye *et al*. (2019) conducted an experimental study on cyclically-damaged steel concrete composite joints subjected to fire.

As previously mentioned, CFST members can be employed in buildings as beams, columns, and beam-columns. A lot of research related to the composite beam-to-CFST column joints has been conducted in recent years. However, only one research related to composite CFST beam-to-column joints has been implemented by Eom *et al.* (2019). This research only focus on the behavior of composite joints having CFST beam connected to steel column but not concrete column. Additionally, conventionally welded joints are inconvenient for transportation and erection in constructing a framed structure.

This paper aimed to introduce a new joint, which is called the composite CFST beam-concrete column joint that is more convenient for transportation and erection in constructing a framed structure than conventionally welded joints. An experimental investigation was conducted to access the structural response of this composite joint. A 3D FE model was developed to model this composite joint utilizing a nonlinear inelastic analysis. Parametric studies that consisted of steel box beam thicknesses, concrete compressive strength, steel yield strength, and concrete reinforcement ratios were considered to investigate their effects on the proposed composite joint behavior.

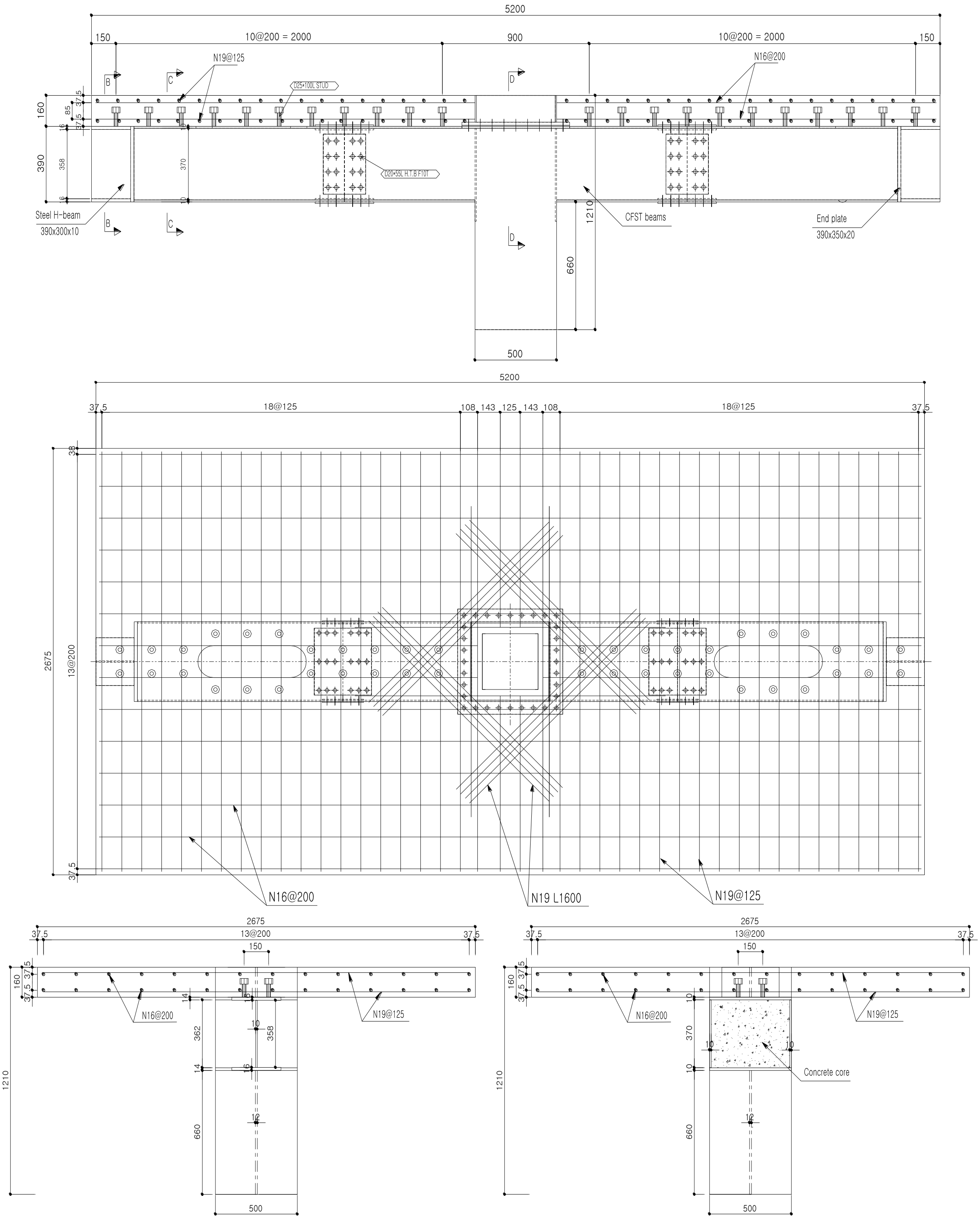

Fig. 1 Detailed geometry of specimen

2. Experimental program

2.1 Specimen design

The composite CFST beam-concrete column joint was designed using Korean standards, such as KBC 2016 (2016), KSCDC 2012 (2012), and KDS 14 31 10:2017 (2017). A detailed design of this joint is displayed in Fig. 1 and Table 1.

In this proposed joint, the main components are the steel H-beam, CFST beams, reinforced concrete columns, and reinforced concrete slabs. The steel H-beam was the build-

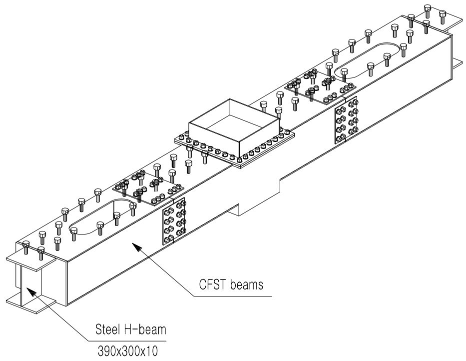

Fig. 2 3D view of the joint

Fig. 3 Specimen preparation

up section, and it was welded with the CFST beam, which included a rectangular steel hollow section and a concrete infill. In the reinforced concrete slab, the main reinforcing bars of N16 were located along the longitudinal direction, and the N19 bars were placed at the transverse direction to prevent longitudinal splitting of the slab. These reinforcing bars were installed in two layers in the slab. In addition, in order to avoid the stress contribution, N19 diagonal bars were installed at the connection between the CFST beams and the concrete column. In the reinforced concrete column, 16N29 bars were employed as main reinforcing bars, and the N10 bars were used for stirrup with spacing of 150 mm. It is noteworthy to mention that two splices shown in Figure 1 were employed in order for more convenience with the erection and transportation of this proposed joint.

A 3D view of this joint is presented in Fig. 2. The steel H-beams were welded with CFST beams using end plates. Two holes, which were symmetrical across the concrete column, were utilized for the concrete casting filling inside the CFST beams. The test specimen was designed so that it could reproduce the joint in a real framed structure. It is noted that the steel H-beams were placed at the positive moment areas, and the CFST beams were located at the negative moment areas in the real framed structure. The reason for this design is to enhance the ultimate load-carrying capacity at the negative moment region and save material at the positive moment area of the framed structure. In addition, both the steel-H beams and CFST beams were connected with the reinforced concrete slab using shear connectors of M25 so the full composite action between them could be obtained. The preparation of the specimen is shown in Fig. 3.

2.2 Material properties

In this study, SM490 steel was employed for all steel components that consisted of the steel box beam, steel H-beam, and the end plates, and SD500 steel was utilized for the rebar in the reinforced concrete slab and the reinforced concrete column of the proposed joint. The material properties of all the steel components were determined by the tensile coupon tests using a displacement controlled testing machine according to the Korean Standard KS D 3515:2014 (2014).

For the material properties of the concrete used in the reinforced concrete slab and the reinforced concrete column of the joint, the concrete compressive strength at 28 days after casting was identified based on the cylinder compression tests according to Korean Standard KS F 2405 (2010), and the concrete tensile strength was determined based on the splitting cylinder tests. The material properties of the steel and the concrete are indicated in Table 2, and the stress-strain curve of the concrete in compression is described in Fig. 4.

2.3 Experimental setup

Fig. 5 represents the test set-up of the proposed joint. A hydraulic jack with a loading capacity of 5,000 kN was employed to impose a vertical load on top of a concrete column. Before testing, the set-up and performance of the components and instrumentation were checked by applying a small load of about 10% of the predicted ultimate load of the specimen. The test specimen was unloaded and reloaded, and the deformation was monotonically increased until no further loading could be sustained by the specimen. The test was carried out using the displacement-control with a loading rate of 2 mm/minute.

2.4 Instrumentation

Fig. 6 reveals the instrumentation layout of the test specimen. These instrumentations include a Linear Variable Displacement Transducer (LVDT) and strain gauges. An LVDT was employed to measure the mid-span displacement, and the strain gauges were used to measure the strain in structural steel, concrete slabs, and concrete columns at different locations of the specimen to evaluate the structural performance and the behavior of the proposed joint.

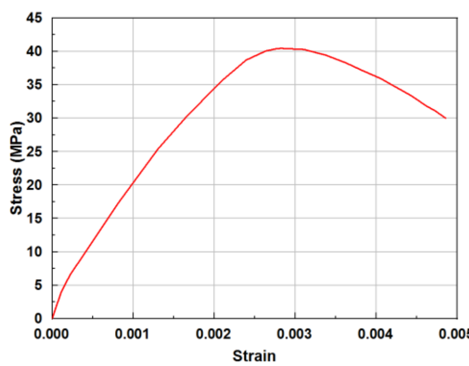

Fig. 4 Stress-strain relationship of concrete cylinder

Fig. 5 Test set-up

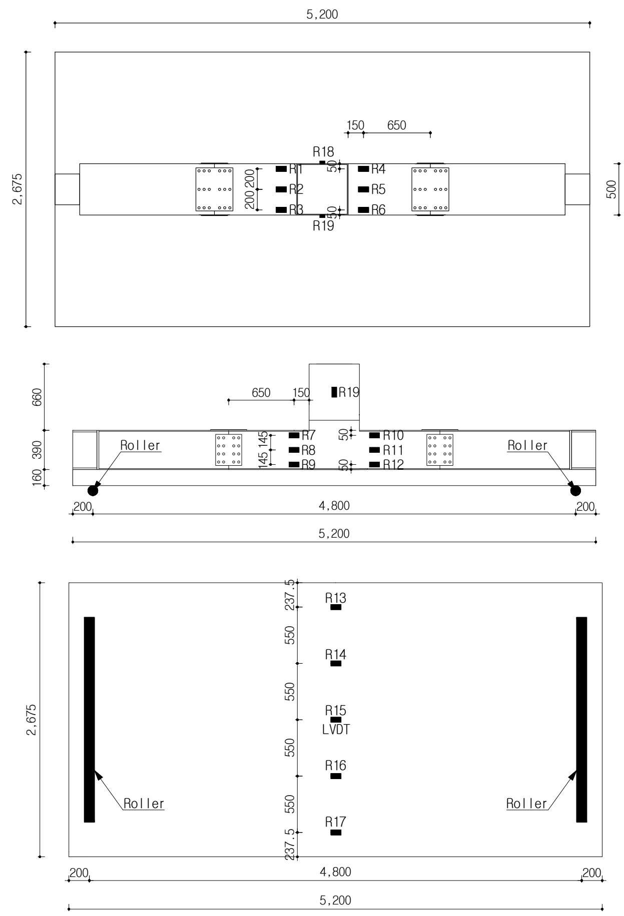

Fig. 6 Instrumentation layout

In order to measure the strains in the structural steel, 12 strain gauges were attached to the CFST beams near the locations where high-stress levels were expected. In addition, five and two strain gauges were employed to measure the strains in the concrete slab and the concrete column, respectively.

2.5 Experimental results

The vertically applied load-mid-span displacement response of the proposed joint, is indicated in Fig. 7, and its typical failure mode is displayed in Fig. 8. The ultimate load of this joint was 1753 kN. It is observed in Fig. 7 that after reaching a load of 1753 kN, the applied load suddenly dropped. The reason may be due to local failure. Especially, it can be seen from Figure 8b that after the test was stopped, outward buckling occured in the steel box beam near the concrete column. Although the specimen was tested symmetrically, the outward buckling that occured in the steel box beam on the left side was much greater than that on the right side. This may be due to the test set up. In addition, the first crack occurred near the mid-span of the slab bottom of the specimen at a loading of 170 kN. At the end of the test, cracks occured around the concrete column's surface and propagated towards the concrete slab edges, which followed an inclined pattern, as presented in Fig. 8(c).

Fig. 9 shows the load-strain responses in the top and lateral faces of the steel box beam, in the lateral faces of concrete column, and in the bottom of the concrete slab of the specimen. From this figure, it was proven that the strains on the left side of the steel box beam were greater than those on the right side. It is also noteworthy from Fig. 9 that the strains in the steel box beam remarkably exceeded the yield strain obtained from the tensile tests' results. It is apparent that there was the occurrence of the yielding of webs and flanges of the steel box beam.

3. Finite element analysis

The commercially available software, ABAQUS (2014), was employed to simulate the composite CFST beam – concrete column joint. A 3D FE model was developed to investigate the proposed joint response. The explicit method was employed to avoid numerical convergence difficulties and reduce the computational time, since the contacts utilized in this joint were complicated. A general layout of the FE model is described in Fig. 10.

3.1 Element type and mesh

In the present study, the eight-node solid elements (C3D8R) were utilized to model the concrete slab, concrete infill, and concrete column of the joint.

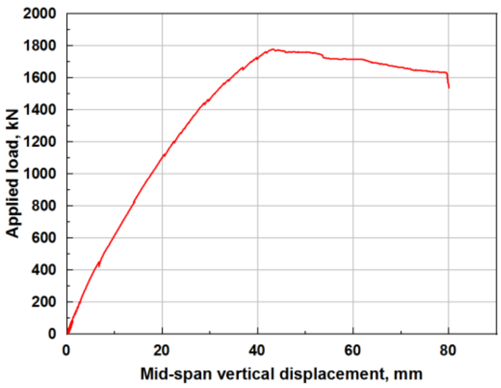

Fig. 7 Load – displacement response of the specimen

(a) Deformation of the specimen

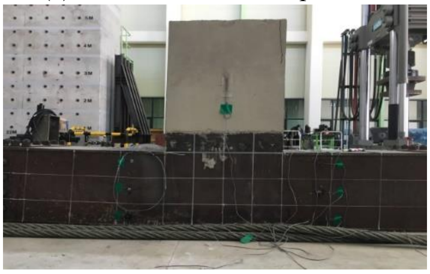

(b) Local buckling of the steel box beam

(c) Crack pattern in concrete slab

Fig. 8 Failure mode of the specimen

The four-node shell elements (S4R) were used to simulate the steel box beam and steel H-beam, because this element type is the most suitable for thin-walled steel structures (Vu *et al*. 2019a, 2019b, Truong *et al*. 2019, Jo *et al*. 2020, Kong *et al*. 2020, etc.). For modeling the rebar in the concrete slab, the four-node quadrilateral surface elements (SFM3D4) were employed to model the longitudinal and transverse rebar using the REBAR option. In addition, three-dimensional truss elements (T3D2) were employed to model the diagonal rebar. Finally, rigid elements (R3D4) were utilized to model the loading pad.

In order to obtain a suitable mesh and provide reliable results, a sensitivity analysis was performed. Based on the analysis results, it was revealed that a mesh size of 50 mm was a reasonable mesh, and it was employed for all the case studies. The FE mesh adopted for the composite joint is presented in Fig. 11.

3.2 Material models

Regarding the concrete model, the concrete damaged plasticity (CDP) model was used for the concrete slab and the concrete infill, because it can capture both the cracking and crushing failures of the concrete.

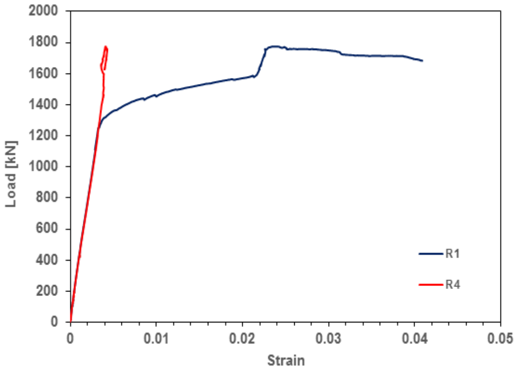

(a) Locations of R1 and R4

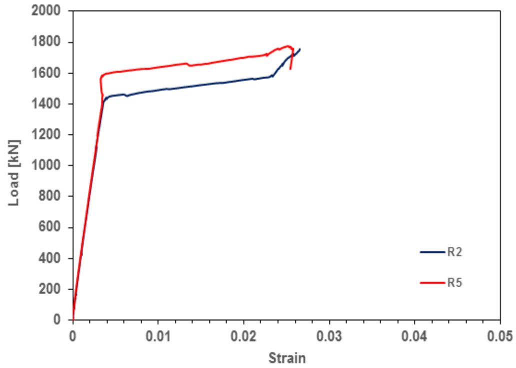

(b) Locations of R2 and R5

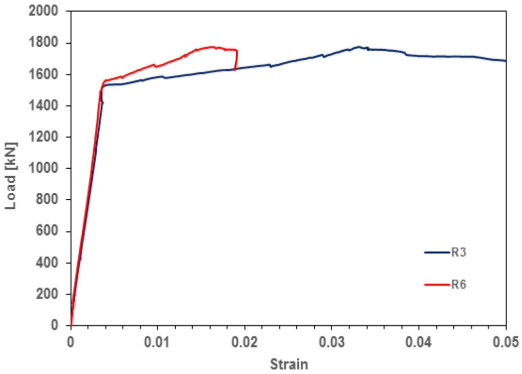

(c) Locations of R3 and R6

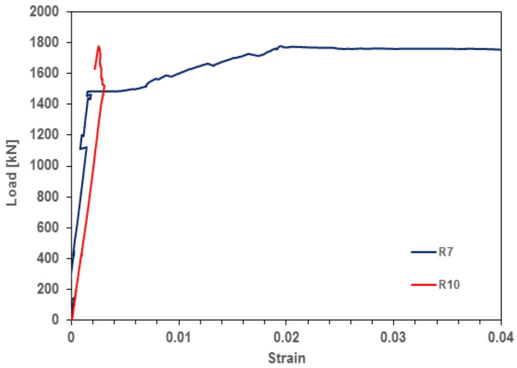

(d) Locations of R7 and R10

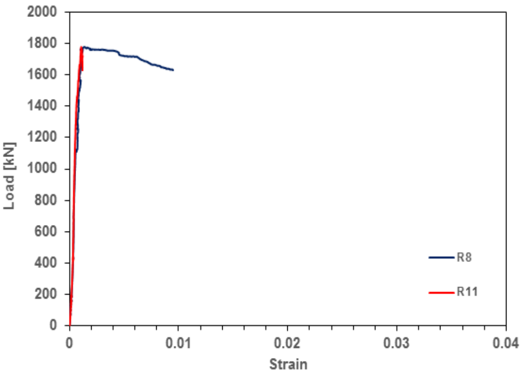

(e) Locations of R8 and R11

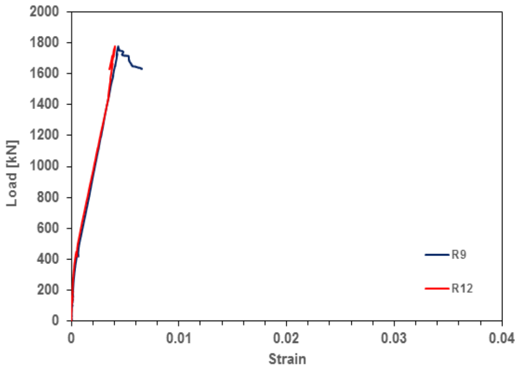

(f) Locations of R9 and R12

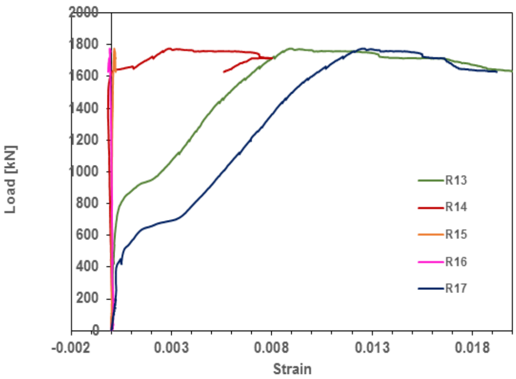

(g) Locations of R13, R14, R15, R16, and R17

Fig. 9 Load-strain response at various locations of the specimen

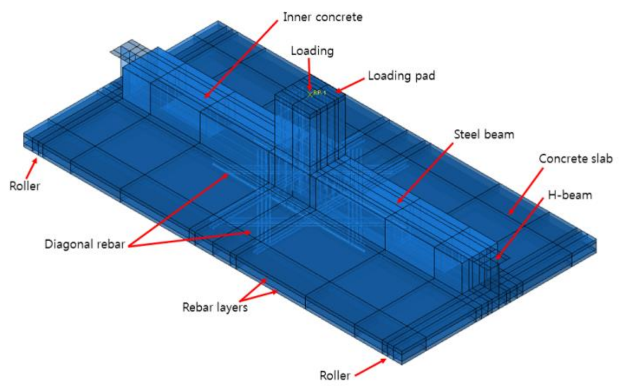

Fig. 10 General layout of the FE model of the composite joint

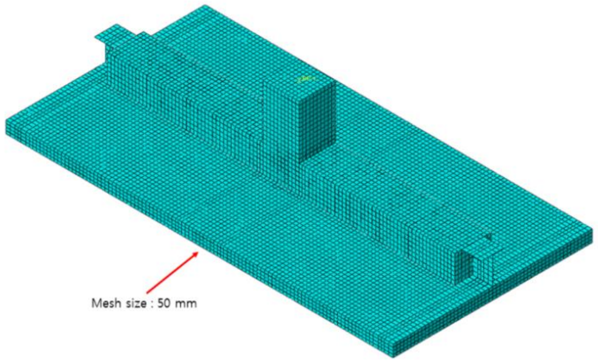

Fig. 11 FE mesh of the composite joint

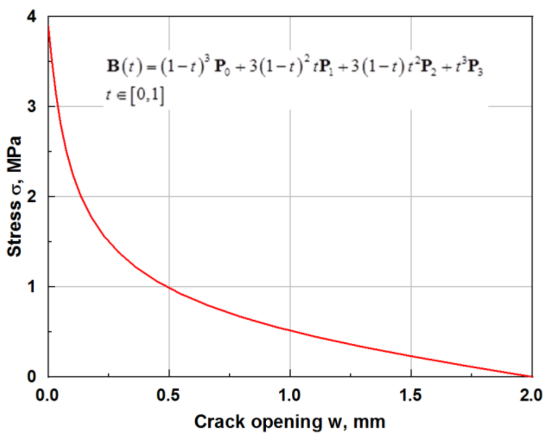

Fig. 12 Tension stiffening model based on the cubic Bézier curve

The stress-strain curve taken from the compressive cylinder test was utilized to simulate the concrete in compression, which is shown in Fig. 4. To model the concrete in tension, the stress-displacement curve was employed to simulate the brittle behavior of the concrete instead of the stress-strain relationship. The concrete tensile model adopted by Kim and Nguyen (2010, 2012) was used, and it is presented in Fig. 12. The stress-displacement behavior of the tensile concrete was based on the cubic

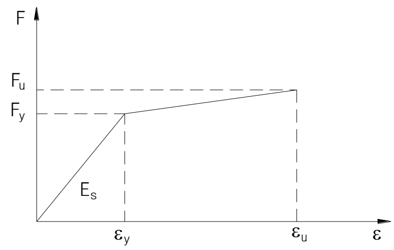

Fig. 13 General stress-strain relationship of steel material used in this study

Bézier curve with an actual crack opening of 1mm. The tensile damage model was taken into consideration based on Kim and Nguyen (2010, 2012). The compressive damage was not considered, because the failure mode achieved from the test was due to concrete cracking.

Regarding the steel model, the bi-linear stress-strain relationship was employed, and it is displayed in Fig. 13. The yield strength F_y, yield strain ε_y, ultimate strength F_u, and the ultimate strain ε_u were taken from tensile test results.

3.3 Contact and constraint conditions

To simulate the contact interaction between various components of the proposed joint, a general contact algorithm was employed. In the current analysis, general contact was imposed for contact between the concrete and the steel with a friction coefficient of 0.1 as a hard contact option. Two contact pairs were defined in the model, which include (1) a steel box beam and a concrete column and (2) a concrete infill and a steel box beam. In addition, to simulate the interaction between the concrete slab and the reinforcing bars, an embedded constraint was employed. In this constraint, the reinforcing bars played the role of an embedded region, and the concrete slab played the role of a host region in order to make a perfect bond between them.

On the other hand, the TIE constraints were employed to simulate the interaction between the steel beams and the concrete slab as well as between the loading pad and the concrete column. It was noted that all the beam components consisting of steel H-beams, end plate, steel box beams, were assembled together.

3.4 Loading and boundary conditions

The simply supported boundary condition was imposed on the upper face of the concrete slab at both ends based on the test set-up. The vertically applied load was imposed on the structure through the reference point located at the top center of the loading pad. The displacement control method, which had a loading rate of 2 mm/min taken from the actual test, was employed in the model using the smooth step amplitude available in the Abaqus/explicit.

3.5 Model verification

To demonstrate the accuracy of the developed FE model, the results obtained from this model were compared to the experimental results presented in Section 2. Fig. 14

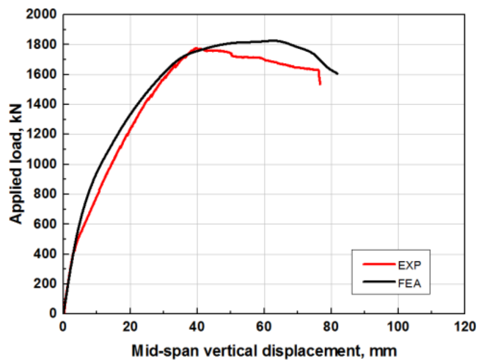

Fig. 14 Comparison of load-displacement curves between FEA and experimental results

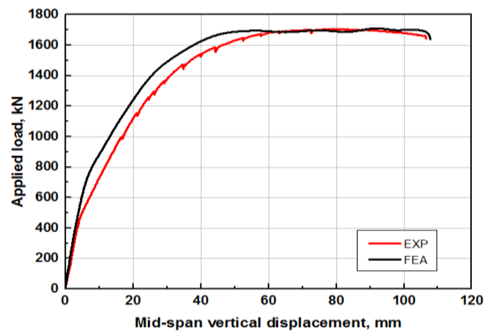

Fig. 15 Comparison of load-displacement curves between FEA and experimental results

illustrates the comparison of load-displacement responses of the ultimate load between the FEA and the experimental results of the composite CFST beam-concrete column joint. It was observed that a good agreement could be obtained between the FEA and the test results. In addition, a similar result was withdrawn from the comparison between the FEA and the test of the composite CFST beam-steel column joint (Eom *et al*. 2019) as presented in Fig. 15.

On the other hand, as illustrated in Figs. 16 and 17, the developed FE model can also accurately predict the failure mode for both the composite CFST beam-concrete column and the composite CFST beam-steel column joints, respectively. Therefore, it was concluded that the developed FE model provided accurate results, and it can capture the real behavior of the composite CFST beam-concrete column joint.

4. Parametric studies

A comprehensive investigation of the effect of parametric studies, which consisted of the steel box beam thickness, concrete compressive strength, steel yield strength, the reinforcement ratio, and the reinforcement spacing in a slab, on the response of composite CFST beam-to-concrete column joints was conducted. The FE model validated by the test result was employed for this investigation.

4.1 Effect of flange thickness of steel box beam

To investigate the effect of the flange thickness of the steel box beam, various flange thicknesses were considered, and they are presented in group 1 in Table 3. The thicknesses of 2.26, 3.76, and 4.99 mm were the minimum values corresponding to the slender, non-compact, and compact flanges of the steel box, which were computed based on the requirement of the KSCDC 2012 (2012). Fig. 18 represents the load-displacement curves of the joint corresponding to various flange thicknesses. It was observed from this figure that there was a significant effect of the flange thickness on the load-displacement response of the joint. For example, it appears in Fig. 18 that when the flange thickness was changed from 2.26 mm (slender flange) to 3.76 mm (non-compact flange), the percentage increase in the ultimate load calculated was 11.45%. When the flange thickness increased from 3.76 mm to 4.99 mm, 8 mm, and 10mm, the ultimate load increased by 5.54%, 7.67%, and 9.23%, respectively.

4.2 Effect of web thickness of steel box beam

The influence of the web thickness of the steel box beam on the response of the proposed joint was also investigated by changing the web thickness, which is illustrated in group 2 in Table 3. The minimum thicknesses for the non-compact and compact webs of the steel box were 3.37 mm and 5.62 mm, respectively. The load-displacement curves of the joint with various web thicknesses are illustrated in Fig. 19. It was observed that the influence of the web thickness of the steel box beam on the ultimate load of the proposed joint was small. The maximum difference in the ultimate load was only 4.8%, which was obtained by calculating the cases of the steel box beam with web thicknesses of 8 mm and 10 mm.

4.3 Effect of concrete compressive strength

The effects of compressive strengths of the concrete infill and the concrete slab on the behavior of the proposed joint were examined. The concrete compressive strength was changed from 30 to 80MPa, which is shown in Groups 3 and 4 in Table 3. The stress-strain relationship of the concrete in compression with respect to various compressive strengths was identified based on EC2 [28].

4.3.1 Effect of compressive strength of concrete slab

To determine the influence of the concrete slab compressive strength on the behavior of the proposed joint, the concrete infill compressive strength was fixed at 40.45 MPa, and the concrete slab compressive strength was changed from 30 to 80 MPa. Fig. 20 reports the load-displacement relationships for various compressive strengths of the concrete slab. It was observed that the concrete slab compressive strength affected the ultimate strength of the composite joint. Especially, the ultimate strength linearly increased with respect to an increase of the compressive strength of the concrete slab, which is shown in Fig. 21.

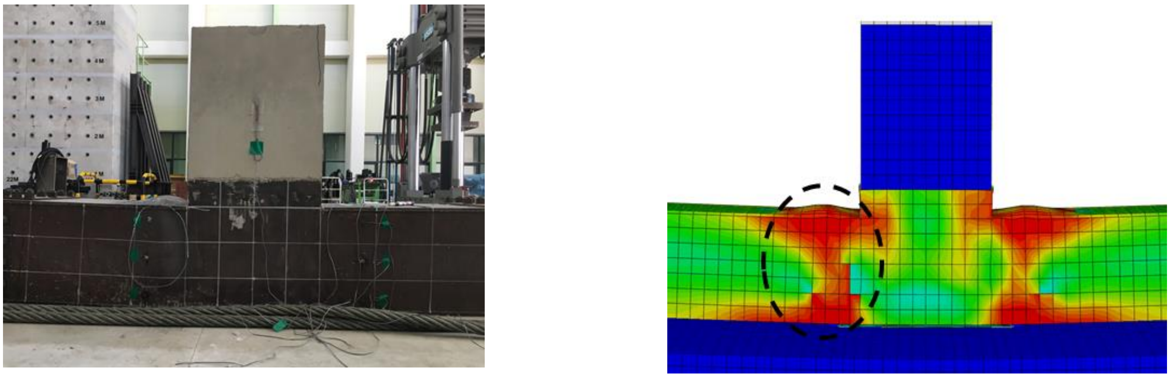

(a) Plastic strain and local buckling of the flange and web of steel box beam

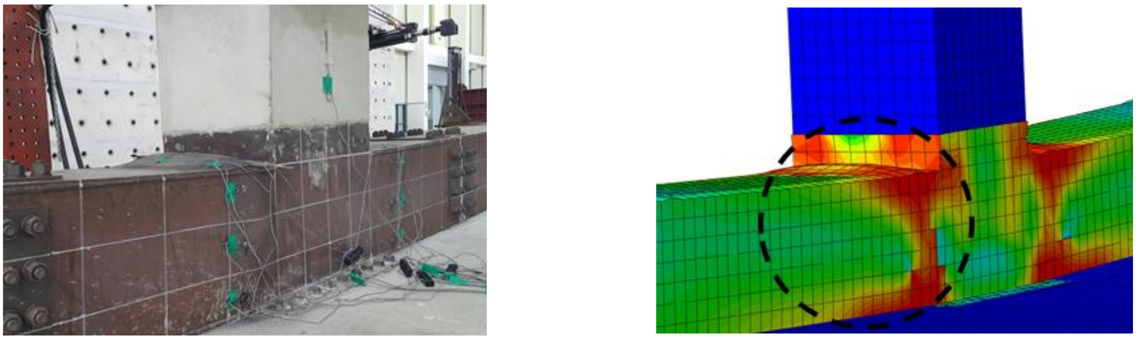

(b) Crack of concrete slab

Fig. 16 Comparison of failure modes between FEA and experimental results

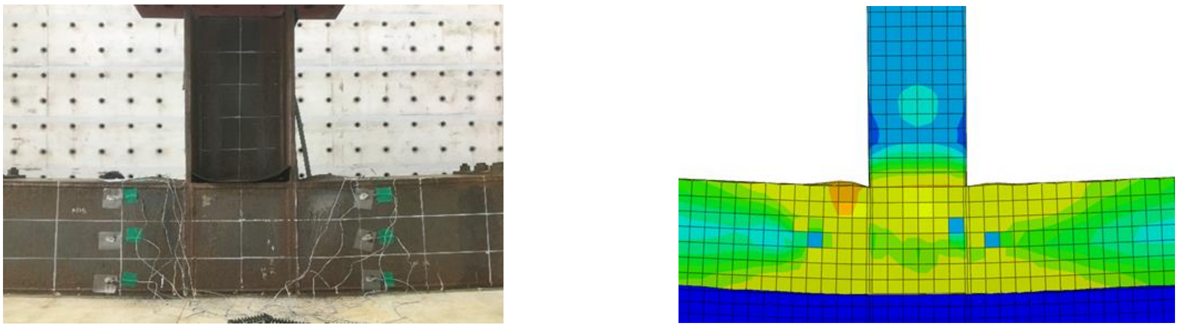

(a) Plastic strain and local buckling of the flange and web of steel box beam

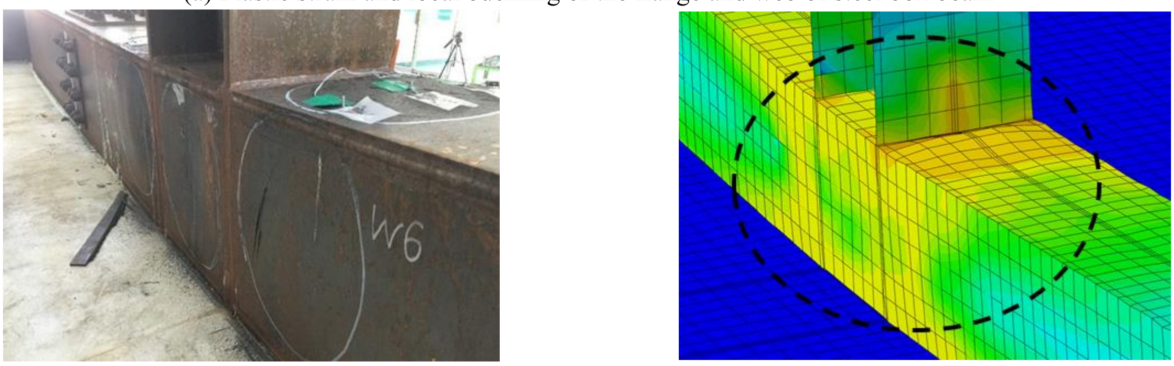

(b) Crack of concrete slab

Fig. 17 Comparison of failure modes between FEA and experimental results

Table 3 Geometric and material properties of composite CFST beam-to-steel column joint used in the parametric study

Group	Composite joint	b_{sbb} x tf (mm)	h_{sbb} x tw(mm)	f'_{c1} (MPa)	f'_{c2} (MPa)	F_y (steel beam) (MPa)	Reinforcement ratio	Reinforcement spacing (mm)
1	CJ-1	500 x 2.26	370 x 8	40.45	40.45	421 (560)	14N16	200
	CJ-2	500 x 3.76	370 x 8	40.45	40.45	421 (560)	14N16	200
	CJ-3	500 x 4.99	370 x 8	40.45	40.45	421 (560)	14N16	200
	CJ-4	500 x 8	370 x 8	40.45	40.45	421 (560)	14N16	200
	CJ-5	500 x 10	370x 8	40.45	40.45	421 (560)	14N16	200
2	CJ-6	500 x 10	370 x 3.37	40.45	40.45	421 (560)	14N16	200
	CJ-7	500 x 10	370 x 5.62	40.45	40.45	421 (560)	14N16	200
	CJ-8	500 x 10	370 x 7	40.45	40.45	421 (560)	14N16	200
	CJ-9	500 x 10	370 x 8	40.45	40.45	421 (560)	14N16	200
	CJ-10	500 x 10	370 x 10	40.45	40.45	421 (560)	14N16	200
3	CJ-11	500 x 10	370 x 8	30	40.45	421 (560)	14N16	200
	CJ-12	500 x 10	370 x 8	40	40.45	421 (560)	14N16	200
	CJ-13	500 x 10	370 x 8	50	40.45	421 (560)	14N16	200
	CJ-14	500 x 10	370 x 8	60	40.45	421 (560)	14N16	200
	CJ-15	500 x 10	370 x 8	70	40.45	421 (560)	14N16	200
	CJ-16	500 x 10	370 x 8	80	40.45	421 (560)	14N16	200
4	CJ-17	500 x 10	370 x 8	40.45	30	421 (560)	14N16	200
	CJ-18	500 x 10	370 x 8	40.45	50	421 (560)	14N16	200
	CJ-19	500 x 10	370 x 8	40.45	60	421 (560)	14N16	200
	CJ-20	500 x 10	370 x 8	40.45	70	421 (560)	14N16	200
	CJ-21	500 x 10	370 x 8	40.45	80	421 (560)	14N16	200
5	CJ-22	500 x 10	370 x 8	40.45	40.45	235 (340)	14N16	200
	CJ-23	500 x 10	370 x 8	40.45	40.45	275 (410)	14N16	200
	CJ-24	500 x 10	370 x 8	40.45	40.45	355 (490)	14N16	200
6	CJ-25	500 x 10	370 x 8	40.45	40.45	421 (560)	14N10	200
	CJ-26	500 x 10	370 x 8	40.45	40.45	421 (560)	14N13	200
	CJ-27	500 x 10	370 x 8	40.45	40.45	421 (560)	14N16	200
	CJ-28	500 x 10	370 x 8	40.45	40.45	421 (560)	14N19	200
	CJ-29	500 x 10	370 x 8	40.45	40.45	421 (560)	14N22	200
7	CJ-30	500 x 10	370 x 8	40.45	40.45	421 (560)	14N16	100
	CJ-31	500 x 10	370 x 8	40.45	40.45	421 (560)	14N16	150
	CJ-32	500 x 10	370 x 8	40.45	40.45	421 (560)	14N16	200
	CJ-33	500 x 10	370 x 8	40.45	40.45	421 (560)	14N16	250
	CJ-34	350 x 14	370 x 8	40.45	40.45	421 (560)	14N16	300

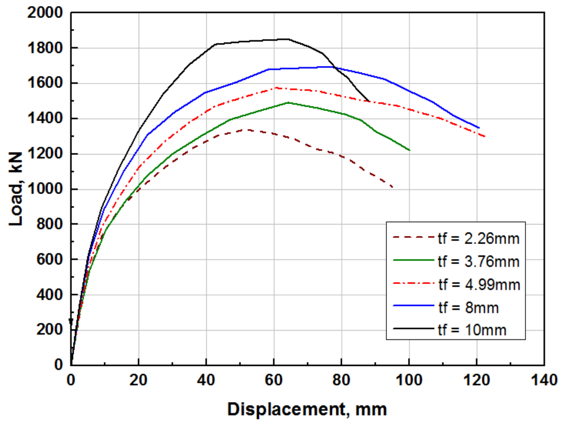

Fig. 18 Load-displacement response of the composite joint for various flange thicknesses of the steel box beams

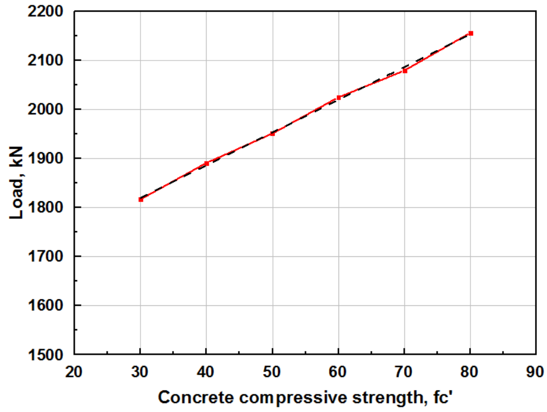

Fig. 21 Relationship between load-compressive strength of the concrete slab

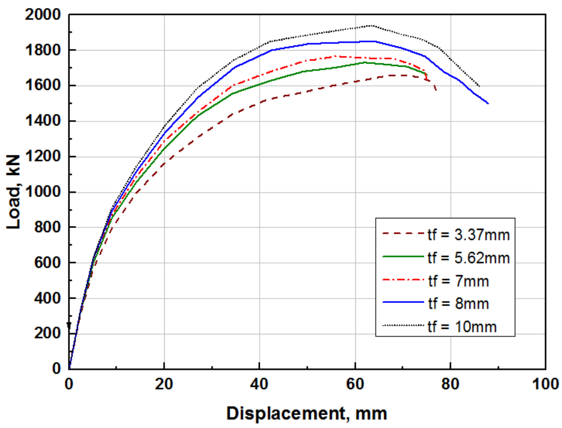

Fig. 19 Load-displacement response of the composite joint for various web thicknesses of the steel box beams

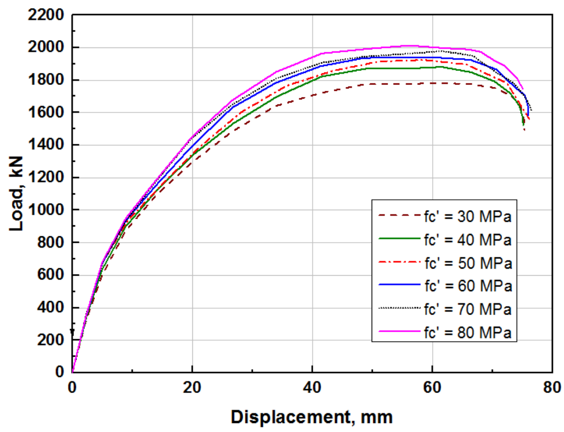

Fig. 22 Load-displacement response for the composite joint for different compressive strengths of concrete infill

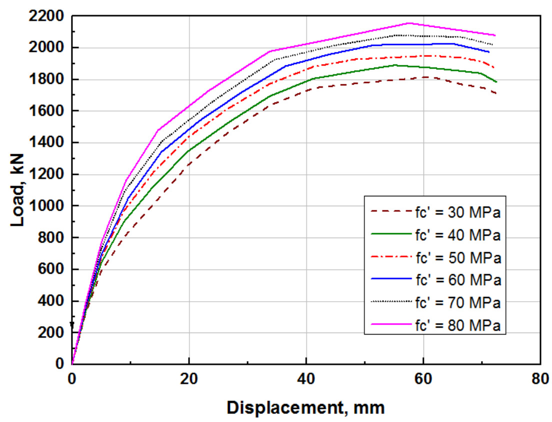

Fig. 20 Load-displacement response of the composite joint for different compressive strengths of concrete slab

4.3.2 Effect of compressive strength of concrete infill

To investigate the effect of the concrete infill compressive strength on the behavior of the proposed joint, the concrete slab compressive strength was fixed at 40.45 MPa (test value), and the concrete infill compressive strength was varied from 30 to 80 MPa. Figure 22 displays the comparison of the load-displacement curves of the joint with the various compressive strengths of the concrete infill. From this figure, only a slight effect of the concrete infill on the ultimate strength of the composite joint was observed.

4.4 Effect of yield strength of steel

The influence of the steel box beam yield strength on the performance of the proposed joint indicated in Group 5 in Table 3 was examined. Only the yield strength of the steel box beam was changed from 235 to 375 MPa, whereas the yield strength of the steel-H beam was fixed. Fig. 23 represents the load-displacement responses of the joint with various steel box yield strengths. This figure shows that the steel beam yield strength does not have any effect on the initial stiffness of the joint. However, at higher loads, steel beams with higher yield strengths exhibited higher stiffness. In addition, the ultimate strength of the composite joint increased by 4.7% and 14% when the yield strength of steel beams increased from 235 MPa to 275 and 355 MPa, respectively.

4.5 Effect of reinforcement ratio

The influence of the reinforcement ratio on the load-displacement responses of the proposed joint is shown in Figure 24. Six different diameters of reinforcing bars of N10, N13, N16, N19, and N22 corresponding to the reinforcement ratios of 0.51, 0.87, 1.31, 1.85, and 2.49% were taken into consideration in the parametric study. It is apparent from this figure that there is a significant effect of the reinforcement ratio on the load-displacement response of the joint. However, the ultimate load of the joints only increased slightly as the reinforcement ratio increased. For instance, when the reinforcement ratio increased from 0.51 to 0.87, 1.31, 1.85, and 2.49%, the ultimate load of the composite joints increased 6.8, 6.13, 5.1, and 2.51%, respectively. It is clear that the higher the reinforcement ratio is, the lower their effect on the ultimate load.

4.6 Effect of reinforcement spacing

The reinforcement spacing was varied from 100 mm to 300 mm, which is illustrated in Group 7 in Table 3, to investigate the effect of spacing of reinforcing bars in slab on the response of the proposed joint. Fig. 25 presents the load-displacement responses of the proposed joint for the various spacing of the reinforcing bars in a concrete slab. It was observed that an increase in the spacing of the reinforcing bars (up to 250 mm) leads to a significant reduction in the load carrying capacity of the joint. However, a further increase in the spacing of reinforcing bars only had a slight reduction in the load carrying capacity of the joint.

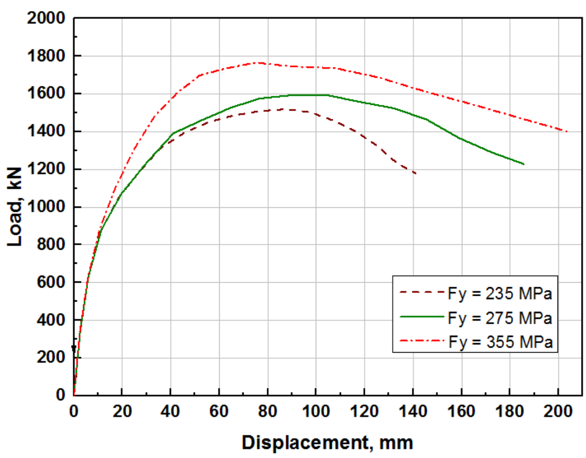

Fig. 23 Load-displacement response of the composite joint for different yield strengths of steel beam

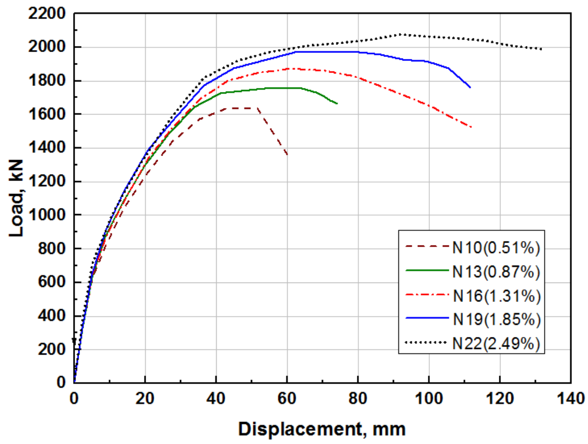

Fig. 24 Load-displacement response for the composite joint for different reinforcement ratios in the concrete slab

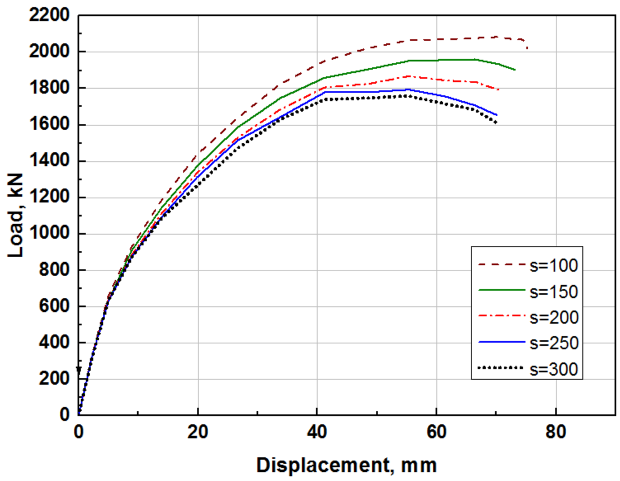

Fig. 25 Load-displacement response for composite joints with different rebars spacing in the concrete slab

5. Conclusions

In the present work, a composite CFST beam-concrete column joint, which is more convenient in transportation and erection than conventionally welded joints, was introduced. Experimental and numerical investigation of this composite joint was performed to evaluate its performance, which resulted in the following conclusions listed below.

- The developed FE model can accurately predict the response of the composite CFST beam-concrete column joint.
- There is a significant effect of the flange thickness of the steel box beam on the ultimate strength of the joint.
- There is a minor effect of the web thickness of the steel box beam on the ultimate strength of the joint.
- The utilization of higher strength steel beams in the joint leads to a higher capacity of this joint.
- Compressive strengths of the concrete infill do not have any remarkable influence on the joint strength.

- The ultimate strength of the joint linearly increases with respect to an increase of the compressive strength of the concrete slab.
- The joint strength only slightly increases as the reinforcement ratio increases. Especially, the higher the reinforcement ratio is, the lower their effect on the ultimate load.
- Increasing the spacing of reinforcing bars to a certain value can significantly reduce the ultimate strength of the joint. However, increasing this spacing any further will only have a slight influence on the joint strength.
- The proposed joint is sufficient and can be utilized for construction.

Acknowledgments

This work was supported by the National Research Foundation of Korea (NRF) grant funded by the Korea government (MSIT)(No. 2018R1A2A2A05018524). This research is funded by Vietnam National Foundation for Science and Technology Development (NAFOSTED) under grant number 107.01-2019.322. This work was also supported by the Natural Science Foundation funded by Department of Education, Anhui Province, China (No. KJ2018A0046); the Natural Science Foundation of Anhui Province, China (No. 1908085ME171); and the Innovation Project for Returnees from Overseas funded by the Department of Human Resources and Social Security, Anhui Province (No. 2019LCX012).

“”

References

ABAQUS (2014), *Analysis user's manual version 6.14*, Dassault Systemes

Ataei, A., Bradford, M.A. and Valipour, H.R. (2015), “Experimental study of flush end plate beam-to-CFST column composite joints with deconstructable bolted shear connectors”, *Eng. Struct.*, **99**, 616-630. https://doi.org/10.1016/j.engstruct.2015.05.012.

Ataei, A., Bradford, M.A. and Valipour, H.R. (2016), “Finite element analysis of HSS semi-rigid composite joints with precast concrete slabs and demountable bolted shear connectors”, *Finite Elem. Anal. Des.*, **122**, 16-38. https://doi.org/10.1016/j.finel.2016.08.003.

Elremaily, A. and Azizinamini, A. (2001), “Experimental behavior of steel beam to CFT column connections”, *J. Constr. Steel Res.*, **57**, 1099-1119. https://doi.org/10.1016/S0143-974X(01)00025-6.

Esfandyary, R., Razzaghi, M.S. and Eslami, A. (2015), “A parametric investigation on the hysteretic behaviour of CFT column to steel beam connections”, *Struct. Eng. Mech.,* **55**(11), 205-228. https://doi.org/10.12989/sem.2015.55.1.205.

Eurocode 2: Design of concrete structures- Part 1-1 (2004), *EUROPEAN COMMITIEE FOR STANDARDIZATION*.

Eom, S.S., Vu, Q.V., Choi, J.H., Park, H.H. and Kim, S.E. (2019), “Flexural behavior of concrete-filled double skin steel tubes with a joint”, *J. Constr. Steel Res.*, **155**, 260-272. https://doi.org/10.1016/j.jcsr.2018.12.012.

Eom, S.S., Vu, Q.V., Choi, J.H., George, P. and Kim, S.E. (2019), “Behavior of composite CFST beam-steel column joints”, *Steel Compos. Struct.*, **32**(5), 583-594. https://doi.org/10.12989/scs.2019.32.5.583.

Guo, L., Wang, J., Wang, W. and Duan, M. (2019), “Seismic evaluation and calculation models of CFDST column blind bolted to composite beam joints with partial shear interaction”, *Eng. Struct.*, **196**, 109269. https://doi.org/10.1016/j.engstruct.2019.06.005.

Han, L.H., Tao, Z., Huang, H. and Zhao, X.L. (2004), “Concrete-filled double skin (SHS outer and CHS inner) steel tubular beam-columns”, *Thin-Wall. Struct.*, **42**, 1329-1355. https://doi.org/10.1016/j.engstruct.2016.09.003.

Han, T.H., Stallings, J.M. and Kang, Y.J. (2010), “Nonlinear concrete model for double-skinned composite tubular columns”, *Constr. Build. Mater.*, **24**, 2542-2553. https://doi.org/10.1016/j.conbuildmat.2010.06.001.

Hassan, M.M, Ramadan, H.M., Naeem, M. and Mourad, S.A. (2014), “Behavior of gusset plate-T0-CCFT connections with different configurations”, *Steel Compos. Struct.*, **17***(*5), 735-751. https://doi.org/10.12989/scs.2014.17.5.735.

Hassan, M.M., Mahmoud, A.A. and Serror, M.H. (2016), “Behavior of concrete-filled double skin steel tube beam-columns”, *Steel Compos. Struct.*, **22**(5), 1141-1162. https://doi.org/10.12989/scs.2016.22.5.1141.

Jordão, S., Simões da Silva, L. and Simões, R. (2014), “Design formulation analysis for high strength steel welded beam-to-column joints”, *Eng. Struct.*, **70**, 63-81. https://doi.org/10.1016/j.engstruct.2014.02.028.

Jo, E.J., Vu, Q.V. and Kim, S.E. (2020), “Effect of residual stress and geometric imperfection on the strength of steel box girders”, *Steel Compos. Struct.*, **34**(3), 423-440. https://doi.org/10.12989/scs.2020.34.3.423.

Kim, S.E. and Nguyen, H.T. (2010), “Finite element modeling and analysis of a hybrid steel-PSC beam connection”, *Eng. Struct.*, **32**, 2557-2569. https://doi.org/10.1016/j.engstruct.2010.04.029.

Kim, S.E. and Nguyen, H.T. (2012), “Evaluation of the connection efficiency of hybrid steel-concrete girder using finite element approach”, *Int. J. Mech. Sci.*, **61**, 8-23. https://doi.org/10.1016/j.ijmecsci.2012.04.008.

Kong, Z., Hong. S., Vu, Q.V., Cao, X., Kim, S.E. and Yu, B. (2020), “New equations for predicting initial stiffness and ultimate moment of flush end-plate connections”, *J. Constr. Steel Res.*, **175**(2020), 106336. https://doi.org/10.1016/j.jcsr.2020.106336.

Korean Standard KS F 2405 (2010), *Korean Standards Association*, Korea.

Korean Structural Concrete Design Code (2012), *Korean Concrete Institute*, Korea.

Korean Standard KS D 3515:2014 (2014), *Korean Standards Association*, Seoul, Korea.

Korean Buidling Code (2016), *Architectural Institute of Korea*, Korea.

Korean Design Standard (2017), *Korean Industrial Standards*, Seoul, Korea.

Li, D., Wang, J., Uy, B., Aslani, F. and Patel, V. (2018), “Analysis and design of demountable circular CFST column-base connections”, *Steel Compos. Struct.*, **28**(5), 559-571. https://doi.org/10.12989/scs.2018.28.5.559.

Loh, H.Y., Uy, B. and Bradford, M.A. (2006), “The effects of partial shear connection in composite flush end plate joints. Part I-Experimental study”, *J. Constr. Steel Res.*, **62**, 378-390. https://doi.org/10.1016/j.jcsr.2005.07.012.

Moon, J., Roeder, C.W., Lehman, D.E. and Lee, H.E. (2012), “Analytical modeling of bending of circular concrete-filled steel tubes”, *Eng. Struct.*, **42**, 349-361. https://doi.org/10.1016/j.engstruct.2012.04.028.

Tao, Z. and Han, L.H. (2006), “Behaviour of concrete-filled double skin rectangular steel tubular beam-columns”, *J. Constr. Steel Res.*, **62**, 631-646.

https://doi.org/10.1016/j.jcsr.2005.11.008.
Thai, H.T. and Uy, B. (2015), "Finite element modelling of blind bolted composite joints", *J. Constr. Steel Res*., **112**, 339-353. https://doi.org/10.1016/j.jcsr.2015.05.011.
Thai, H.T., Uy, B., Yamesri and Aslani, F. (2017), "Behaviour of bolted endplate composite joints to square and circular CFST columns", *J. Constr. Steel Res.,* **131**, 68-82. https://doi.org/10.1016/j.jcsr.2016.12.022.
Thomas, J. and Sandeep, T.N. (2018), "Experimental study on circular CFST short columns with intermittently welded stiffeners", *Steel Compos. Struct*., **29**(5), 659-667. https://doi.org/10.12989/scs.2018.29.5.659.
Truong, V.H., Papazafeiropoulos, G., Pham, V.T. and Vu, Q.V. (2019), "Effect of multiple longitudinal stiffeners on ultimate strength of steel plate girders", *Structures*, **22**, 366-382. https://doi.org/10.1016/j.istruc.2019.09.002.
Tong, L., Huang, X., Zhou, F. and Chen, Y. (2016), "Experimental and numerical investigations on extremely-low-cycle fatigue fracture behavior of steel welded joints", *J. Constr. Steel Res*., **119**, 98-112. https://doi.org/10.1016/j.jcsr.2015.12.015.
Vu, Q.V., Thai, D.K. and Kim, S.E. (2018), "Effect of intermediate diaphragms on the load-carrying capacity of steel-concrete composite box girder bridges", *Thin-Wall. Struct*., **122**, 230-241. https://doi.org/10.1016/j.tws.2017.10.024.
Vu, Q.V., Papazafeiropoulos, G., Graciano, C. and Kim S.E. (2019), "Optimum linear buckling analysis of longitudinally multi-stiffened steel plates subjected to combined bending and shear", Thin-Wall. Struct., 136, 235-245.
https://doi.org/10.1016/j.tws.2018.12.008.
Vu, Q.V., Truong, V.H., Papazafeiropoulos, G., Graciano, C. and Kim S.E. (2019), "Bend-buckling strength of steel plates with multiple longitudinal stiffeners", *J. Constr. Steel Res*., **158**, 41-52. https://doi.org/10.1016/j.jcsr.2019.03.006.
Wang, J., Uy, B. and Li, D. (2018), "Analysis of demountable steel and composite frames with semi-rigid bolted joints", *Steel Compos. Struct*., **28**(3), 363-380. https://doi.org/10.12989/scs.2018.28.3.363.
Wang, J.F., Han, L.H. and Uy, B. (2009), "Behaviour of flush end plate joints to concrete-filled steel tubular columns", *Journal of Constructional Steel Research*. **65** 925-939.
https://doi.org/10.1016/j.jcsr.2008.12.008
Wang, J.F., Han, L.H. and Uy, B. (2009), "Hysteretic behaviour of flush end plate joints to concrete-filled steel tubular columns", *Journal of Constructional Steel Research*. **65** 1644-1663.
https://doi.org/10.1016/j.jcsr.2008.12.008
Waqas, R., Uy, B. and Thai, H.T. (2019), "Experimental and numerical behaviour of blind bolted flush endplate composite connections", *J. Constr. Steel Res*., **153**, 179-195. https://doi.org/10.1016/j.jcsr.2018.10.012.
Yang, C.M. and Kim, Y.M. (2007), "Cyclic behavior of bolted and welded beam-to-column joints", *Int. J. Mech. Sci*., **49**, 635-649. https://doi.org/10.1016/j.ijmecsci.2006.09.022.
Yang, J., Sheehan, T., Dai, X.H. and Lam, D. (2015), "Experimental study of beam to concrete-filled elliptical steel tubular column connections", *Thin-Wall. Struct*., **95**, 16-23. https://doi.org/10.1016/j.tws.2015.06.009.
Yuan, F., Chen, M. and Huang, H. (2019), "Square CFST columns under cylic load and acid rain attack: Experiments", *Steel Compos. Struct.*, **30**(2), 171-183. https://doi.org/10.12989/scs.2019.30.2.171.
Ye, Z., Jiang, S., Heidarpour, A., Li, Y. and Li, G. (2019), "Experimental study on cyclically-damaged steel-concrete composite joints subjected to fire", *Steel Composi. Struct*., **30**(4), 351-364. https://doi.org/10.12989/scs.2019.30.4.351.

BU

NOTATION

b_{sbb} Width of steel box beam
h_{sbb} Depth of steel box beam
E_s Elastic modulus of steel
f_{ck} Cylinder compressive strength of concrete
f'_{c1} Compressive strength of concrete slab
f'_{c2} Compressive strength of concrete infill
f_{tk} Tensile strength of concrete
F_y Yield strength of steel
F_u Ultimate strength of steel
t_f Flange thickness of steel box beam
t_w Web thickness of steel box beam
ε_y Yield strain of steel
ε_u Ultimate strain of steel
ε_c Strain of the peak compressive stress f_{ck}